The American Journal of Pathology, Vol. 175, No. 1, July 2009

DOI: 10.2353/ajpath.2009.080927

Vascular Biology, Atherosclerosis and Endothelium Biology

Complement Factor H Is Critical in the Maintenance of Retinal Perfusion

Peter Lundh von Leithner,* Jaimie Hoh Kam,* James Bainbridge,* Ian Catchpole,† Gerald Gough,† Peter Coffey,* and Glen Jeffery*

From the Institute of Ophthalmology, University College London, and BioPharm CEDD Biology,† GlaxoSmithKline Medicine's Research Centre, Stevenage, Herts, United Kingdom*

Vascular pathologies are known to be associated with age-related macular degeneration. Recently, age-related macular degeneration was associated with a single-nucleotide substitution of the complement factor H (CFH) gene, part of the alternative pathway of the complement system, a critical element in the innate immune response. Such polymorphisms are found in more than 50% of cases of age-related macular degeneration. Here we show that the absence of CFH causes an autoimmune response that targets the vascular endothelium of both the inner and outer retinal vascular networks. In CFH-knockout (*cfh*$^{-/-}$) mice, C3 and C3b, key components of the complement system, are progressively deposited on retinal vessels, which subsequently become restricted and wither, resulting in a reduction of retinal blood supply. This result leads to increased oxygen stress. While such effects are not systemic, these structural changes are mirrored in functional changes with a substantial decline in retinal blood flow dynamics. When the system is challenged functionally by laser-induced choroidal neovascularization, fluorescein leakage was significantly smaller in *cfh*$^{-/-}$ mice compared with controls, likely due to reduced retinal perfusion. These data reveal that in both the presence and absence of exogenous challenge to the innate immune system, CFH is required to maintain normal levels of retinal perfusion. It is likely that C3 and C3b accumulation in the aged CFH-deficient retina is associated with complement-mediated retinal endothelium destruction. ***(Am J Pathol 2009, 175:412–421; DOI: 10.2353/ajpath.2009.080927)***

The association of vascular pathologies with age-related macular degeneration (AMD) is well documented.[1–5] AMD pathogenesis is principally associated with a thickening and reduced flexibility of Bruch's membrane, which leads to a reduction in transport of metabolites and oxidative damages.[6–8] Age-related lipid deposits accumulate under the retina isolating it from its outer blood supply, resulting in geographic atrophy, which can progress to choroidal neovascularization (CNV). The new retinal vessels are fragile and leak, raising the risk of geographic atrophy developing into complete blindness.

Recently, AMD has become associated with a single nucleotide polymorphism of the complement factor-H (CFH) gene, which forms part of the alternative pathway (AP) of the complement system.[9–19] A common single nucleotide polymorphism in the factor H gene is linked with a high risk of developing macular drusen and a predisposition to AMD. CFH blocks the alternative pathway of complement on self-surfaces bearing specific polyanions and binds C-reactive protein, potentially contributing to noninflammatory apoptotic processes. This polymorphism is not lethal, and evolutionarily it may have provided a selective advantage against some pathogen given the binding function of the seventh repeat unit.

CFH is a plasma protein produced by the liver that is an important component of the mammalian complement system, which regulates the alternative pathway of complement activation and protects the host cell from inappropriate complement activation. It acts as a cofactor for complement factor I in the inactivation of the central complement protein C3b to form iC3b. CFH also accelerates the decay of the C3 convertase C3bBb of the alternative pathway, and competes with factor B for binding to C3b.[20] It is a key regulator of innate immunity, and its deficiency can lead to membranoproliferative glomerulonephritis type II[21] and atypical hemolytic uraemic syndrome,[22] two serious diseases affecting the Kidney. The association between AMD-like changes and membranoproliferative glomerulonephritis type II, a renal immune disease linked with AP dysregulation, together with the observation that *cfh*$^{-/-}$ mice spontaneously develop membranoproliferative glomerulonephritis type II,[22] led

Supported by GlaxoSmithKline, UK.

Accepted for publication March 17, 2009.

GSK has no financial interest in the finding related to this study.

Address reprint requests to Glen Jeffery, Institute of Ophthalmology, University College London, Bath Street, London EC1V 9EL, UK. E-mail: g.jeffery@ucl.ac.uk.

Table 1. Antibodies Used for Immunohistochemistry

Experiment	1-year-old cfh$^{-/-}$ (*n*)	1-year-old controls (*n*)	3-month-old cfh$^{-/-}$ (*n*)	Negative controls (*n*)
CFH–C3 section labeling	5	5	5	
C3–Isolectin B4 section labeling	5	5	5	
Choroidal thickness in sections	5	5	5	
NADPH–C3–C3b flatmount labeling	5	5	5	
C3–C3b section labeling	5	5	5	
Non-ocular C3 section labeling	4	4	4	
Fluorescein angiography	6	5	4	
Arteriovenous phase	6	5	4	
CNV fluorescein angiography	5	5		
CNV permeability assay	4	4		2

CFH, complement factor H; CNV, choroidal neovascularization.

us to ask whether C3 deposition due to CFH deficiency predisposes animals to impaired retinal perfusion.

In a previous study,[23] the theory that AP dysregulation due to CFH deficiency would predispose to retinopathy was tested in mice. Aged mice lacking in CFH have also been shown to display structural and functional retinal abnormalities; however, it had been stated that their retinal vasculature was normal.[20] Here we test the more specific hypothesis that absence of CFH principally affects the endothelium of retinal vascular networks causing a constriction and withering of vessels, leading to increased oxygen stress. We use fluorescein angiography and high magnification confocal scanning laser ophthalmoscopy to visualize retinal vascular architecture and perfusion rates in young and aged and *cfh*$^{-/-}$ and wild-type mice. We compared these architectural patterns with localization of C3 deposition. Further, we examine structural differences in retinal vascular architecture between wild-type and knockout mice with their response to laser-induced CNV and its associated leakage, linking anatomical differences with functional responses to injury.

Materials and Methods

Animals

Three-month-old and 1-year-old homozygous CFH-deficient (*cfh*$^{-/-}$) mice (backcrossed onto the C57BL/6 genetic background for more than 10 generations)[20,22] and age-matched normal C57BL/6 mice were housed in a temperature-controlled environment with a 12-hour day (160 lux)–night cycle and maintained on a normal lab diet.

Mice were anesthetized (0.75 ml ketamine, 0.5 ml medetomidine hydrochloride [Domitor], 0.75 ml sterile water, at 0.2 ml/100 g, i.p. supplemented as necessary) and their pupils were dilated with topical 1% tropicamide and 2.5% phenylephrine hydrochloride 10 to 15 minutes before scanning laser ophthalmoscope (cSLO) imaging. Before each image sequence, drops of hydroxypropyl methylcellulose (0.3%) were placed on the eye to prevent drying.

All experimental procedures complied with and were performed under the United Kingdom Animals (Scientific Procedures) Act 1986. Table 1 provides the number of animals used in each of the procedures listed below.

Induction of Choroidal Neovascularization

Eyes of 1-year-old *cfh*$^{-/-}$ mice ($n = 10$) and age-matched normal C57BL/6 mice ($n = 10$) were exposed to laser photocoagulation for induction of experimental CNV. Mice were anesthetized with ketamine hydrochloride (100 mg/kg body weight), and the pupils were dilated with 1% tropicamide. Dye laser photocoagulation was performed using a diode-pumped, frequency doubled 532 nm laser (Oculight GLx Laser System, Iridex Corporation, Mountain View, CA) attached to a slit lamp, and a coverslip was applied to the cornea to view and focus on the retina. Exposure (532 nm, 200 mW during 200 ms, and 100 μm spotsize) was performed on both eyes of each animal ($n = 5$ per group) by an operator masked to its genetic identity. Three laser spots were generated in a peripapillary distribution in a standardized fashion, two to three disk diameters from the optic nerve. The lesions were located at 60-degree peripapillary distributed intervals, centered on the optic nerve at around 1 mm from the optic nerve. The morphological end point was identified as the appearance of a cavitation bubble, a sign associated with the disruption of Bruch's membrane. Laser spots that did not result in the formation of a bubble were excluded from the studies.

Retinal Imaging

High resolution and high contrast fluorescein angiographs were acquired *in vivo* using a modified confocal cSLO (Heidelberg Retina Angiograph, Heidelberg Engineering, Germany) where the pinhole diameter had been reduced to 100 μm to improve axial resolution, and the laser power increased to improve signal-to-noise ratio. Power at the mouse pupil was measured to be 1400 μW at 488 nm. The mouse was fitted with a specially designed plano-concave contact lens and optical power was provided using a $\times$50 microscopic lens with an extra-long working distance, which improved optical resolving power and allowed detection of microcapillary structures as small as 3 μm in diameter.

Fluorescein angiography images were recorded using an emission cut-off filter with the edge of the barrier (value of 50% transmission) at 498 nm. Image sequences of 125 fluorescence images were captured and exported as AVI files, and an ensemble-averaging program, written and implemented in MatLab (Mathworks, Natick, MA), was used to increase dynamic range and signal-to-noise ratio.

Tomographic image stacks were recorded where the axial plane was sequentially moved at 15-μm intervals, vitreal-to-scleral and central-to-peripheral to visualize retinal vasculature from the primary plexus through to the outer plexus. All image sequences were captured at 8.9 Hz, 10° field-of-view, and were digitized as 8-bit, 768 × 768-pixel image files, resulting in a lateral image resolution of 1.2 μm/pixel. Axial resolution in the mouse eye was measured to be 5 to 8 μm.

In Vivo *Fluorescein Angiography*

Fluorescein angiography was performed on aged CFH-deficient mice ($n = 6$), age-matched controls ($n = 5$), and 3-month-old *cfh*$^{-/-}$ ($n = 4$) Following intraperitoneal injection of fluorescein in an aqueous solution (0.2 ml 5% fluorescein sodium) it appears in the retina within 5 to 10 seconds when imaged with the argon laser source of the cSLO. Within 5 to 10 minutes of administration scattering occurs due to leakage of fluorescein through the endothelium into surrounding tissues and interstitial ocular space.

The arteriovenous perfusion phase was determined in al animals from video sequences (10Hz) started at time of injection by subtracting the time it took to fill veins from that of the arteries.

Quantification of CNV Leakage

One-year-old *cfh*$^{-/-}$ ($n = 4$) and age-matched controls ($n = 4$) were anesthetized with ketamin/Dormitor. Choroidal neovascular vessel leakage was quantitated in 1-year-old *cfh*$^{-/-}$ ($n = 4$) and age-matched control retinae ($n = 4$) using fluorescein isothiocyanate (FITC)- and rhodamine-conjugated dextran. Five retinal lesions were made bi-laterally to induce CNV (see method for experimental CNV induction above). Ten days after photocoagulation the mice received intravenous injection of a combination of fluorochrome-conjugated dextrans, which was quantified using a modified protocol for measuring vascular leakage.[24,25]

Fluorescein isothiocyanate-conjugated dextran (10 kDa, Sigma-Aldrich) and rhodamine B isothiocyanate-conjugated dextran (40 kDa, Sigma-Aldrich, Gillingham, Doreset) was dissolved in normal saline sonicated for 5 minutes (50 mg/ml), and filtered through a 5 μm filter. Under deep anesthesia, 50 mg/kg body weight of respective dextran-agent was injected into the tail vein and circulated for 10 minutes. The chest cavity was opened and the left ventricle of the heart cannulated, a blood sample was collected immediately before perfusion, and each mouse was perfused with PBS for 2 minutes (500 ml/kg body weight) at a physiological pressure of 60 mm/Hg to clear the remaining intravascular dextran agent. The blood sample was centrifuged at 7000 rpm for 20 minutes at 4°C, and the supernatant was diluted at 1:1000. Immediately after perfusion, the eyes were enucleated and the retinae and sclera-choroid complex were carefully dissected and collected in separate vials. The tissue was weighed after thorough drying. The dextran-agents were extracted by subsequent incubation of the tissue in 0.4 ml of water for 1 hour at 70°C, followed by homogenization to extract dextran-agents in 0.4 ml of water. Extracts were processed through a 30,000 molecular weight filter (Ultrafree-MC; Millipore, Bedford, MA) at 5000 × *g* for 45 minutes at 4°C. The fluorescence emission of each 200 μl supernatant was measured (FITC-dextran: excitation, 488 nm; emission, 500 to 535 nm; rhodamine-dextran: excitation, 543 nm; emission, 590 to 700 nm), using a spectrofluorometer (FluoStar Optima; BMG Labtech, Germany) with water as a blank. Corrections were made by subtracting the autofluorescence of retinal tissue from mice without dextran-agent injections ($n = 2$). The dye concentration in the extracts was calculated from measured standard curves of FITC- and rhodamine-dextran. For normalization, dextran fluorochrome amount was divided by the retinal weight and by the concentration of FITC-dextran in the plasma.

Histology

Following imaging experiments, rats were deeply anesthetized with sodium pentobarbital (200 mg/kg) and perfused intracardially with 0.1 M/L PBS, followed by 4% paraformaldehyde. Eyes were removed and either prepared for retinal whole mounts (see below) or post-fixed overnight at 4°C. After washing in PBS eyes were cryoprotected in 30% sucrose, the lens removed and frozen in OCT (Tissue Tek) in a dry ice/acetone freezing slurry. Cryostat sections (10 μm) were thaw-mounted onto charged slides.

To obtain whole mounts, retinae were dissected free in 4% paraformaldehyde as follows: Four equidistant cuts were made with microsurgical scissors and the retinae freed from surrounding retinal pigment epithelium (RPE)/choroid using fine forceps. Vitreous was removed by placing circles of fiber-free paper directly onto the surface of the inner retina. Whole mounts were left in 4% paraformaldehyde for a further 10 minutes before washing off the paper (and adherent vitreous) with PBS. When preparing individual retinae in this fashion, the largest cut was always made dorsally (with reference to the remaining superior eyelid). This orientated each specimen such that dorsal and ventral regions were clearly distinguishable when mounting retinae.

Immunohistochemistry

Immunohistochemistry was undertaken on 10-μm thick cryostat sections from eyes fixed in 4% paraformaldehyde. Retinal sections were blocked for 1 hour in 5% normal donkey serum in 0.1 M/L PBS, pH 7.4 with 0.3%

Table 2. Experimental Animal Groups

Antibody	Manufacturer	Dilution
Anti-factor H goat polyclonal	Calbiochem, Merck Bioscience	1:50
Rabbit polyclonal to complement C3	Abcam	1:10
C3b/iC3b/C3c Rat monoclonal to mouse	Hycult biotechnology	1:50
Rabbit polyclonal to C5	Abcam	1:10
Rabbit Polyclonal to C5b-9 (MAC)	Abcam	1:100
Fluorescein conjugated Rat anti-mouse F4/80	Invitrogen	1:100
Alexa Fluor 594 conjugated to isolectin	Invitrogen	1:50

Wherever possible individual animals were used in multiple experiments and eyes harvested bilaterally. All antibodies came from UK suppliers.

Triton X-100, and incubated overnight with primary antibodies, diluted with 1% normal donkey serum in 0.1 M/L PBS with 0.3% Triton X-100. Dilutions of each primary antibody were as shown in Table 2. Primary antibody exposure was followed by washing, and where required, fluorescently conjugated appropriate secondary antibodies (Santa Cruz, Biotechnology, Inc.) made up in the same diluent as the primary and the sections were exposed for 1 hour. Negative controls consisted of both an unrelated isotype matched antibody or omission of the primary antibody. Nuclei were subsequently stained with 4′,6-diamidino-2-phenylindole (1 μl stock solution to 5 ml of 0.1 M/L PBS; Sigma-Aldrich) for 1 minute. Slides were then washed several times 0.1 M/L PBS followed by washes in Tris buffer saline (pH 7.4) and finally mounted in Vectashield (Vector Laboratories, UK).

For NADPH-diaphorase staining, flatmounted retinae were processed according to the modified protocol from.[26] Following the exposure to the fluorescently conjugated primary antibody, the sections were washed and then incubated with medium containing 3% Triton X-100, 0.02% NADPH-tetrasodium salt (Sigma-Aldrich cat. Ref. D-1630), and 0.04% nitroblue tetrazolium (Sigma-Aldrich) in 0.1 M/L PBS for 90 minutes in a 37°C water bath with agitation. The slides were washed and the nuclei stained with 4′,6-diamidino-2-phenylindole for 1 minute and mounted with Vectashield (Vector Laboratories).

To quantify the choroidal thickness in aged $cfh^{-/-}$ retinae its thickness was measured in cryoprotected retinal sections at a distance of around 1.0 mm from the center of the optic nerve head. The value of each retinal thickness was obtained from 10 measurements from 5 sections selected in retinae from each animal group ($n = 5$).

To determine whether C3 deposition was present in other organs 1-year-old $cfh^{-/-}$ mice were perfused with 4% paraformaldehyde in phosphate buffer saline (pH 7.2). Eyes, kidneys, liver, brain, heart, and aorta were removed. Vascular rich areas of the brain (around Circle of Willis) were sectioned at 100 μm using a sledge microtome. Other organs (excluding eyes) were cryoprotected and sectioned at 20 to 30 μm using cryostat. The neural retina and choroid of selected animals were separated and flat-mounted independently.

Sections were viewed and images captured on either a laser scanning confocal microscope (Leica SP2; Leitz, UK) at 8 bit/channel and 1024 × 1024 pixel, or an Epifluorescence bright-field microscope (Olympus BX50F4, Olympus, Japan), where data were captured as 24-bit color images at 3840 × 3072 pixel resolution using Nikon DXM1200 (Nikon, Tokyo, Japan) digital camera.

Statistical Analysis

Differences in the fluorescein angiograms data captured at the primary plexus and the outer plexus in the three groups of animals, aged $cfh^{-/-}$, age-matched control, and young $cfh^{-/-}$ mice, and were statistically quantified. Venous beads in the primary plexus were defined as local constrictions, where the calibre of the vein was reduced by at least 40%, as compared with adjacent sections of the vein. The beads were counted within a 750 μm radius of the optic disk and the data compiled using a one-way analysis of variance. To avoid the influence of lens yellowing on fluorescence emission in aged animals, the quantification of perfusion of the outer plexus vascular bed was based on edge detection, rather than luminance values. Capillary density in the outer plexus was quantified using a simple edge detection analysis where capillaries were counted at successive radial distances from the optic disk and the data presented as number of vessels per linear unit (100 μm). One-way analysis of variance method was used to analyze these data sets. Paired *t*-tests were used to compare knockout with age-matched wild-type populations.

For the evaluation of experimentally induced CNV, the intensity of staining in late-phase (140 to 180 seconds after dye injection) fluorescein angiography was graded by two examiners in a masked fashion. Angiograms were graded as follows: Score 0, no staining; score 1, slightly stained; score 2, moderately stained; score 3, strongly stained, and the score was evaluated by a Wilcoxon signed rank test. When the two scores given for a particular lesion did not coincide, the higher score was used for the analysis.[27] All computation and analysis was performed using MatLab (Mathworks Inc., MA).

Results

Aged $cfh^{-/-}$ retinae show an accumulation of complement C3 in their inner and outer retinal vasculature. Aged wild-type animals possessed normal CFH levels at the RPE/Bruch's membrane interface, but this was absent in both $cfh^{-/-}$ age groups. Complement C3 protein was not detectable by immunohistochemistry in wild-type retinae, but accumulated with age around Bruch's membrane in the CFH-deficient mice (Figure 1, A–F).

Complement C3 protein was absent from the aged wild-type inner and outer retina but was present in mutant animals especially those that were aged (Figure 2, A–F). In the outer retina C3 accumulated with age around Bruch's membrane in $cfh^{-/-}$ animals (Figure 2, D–F).

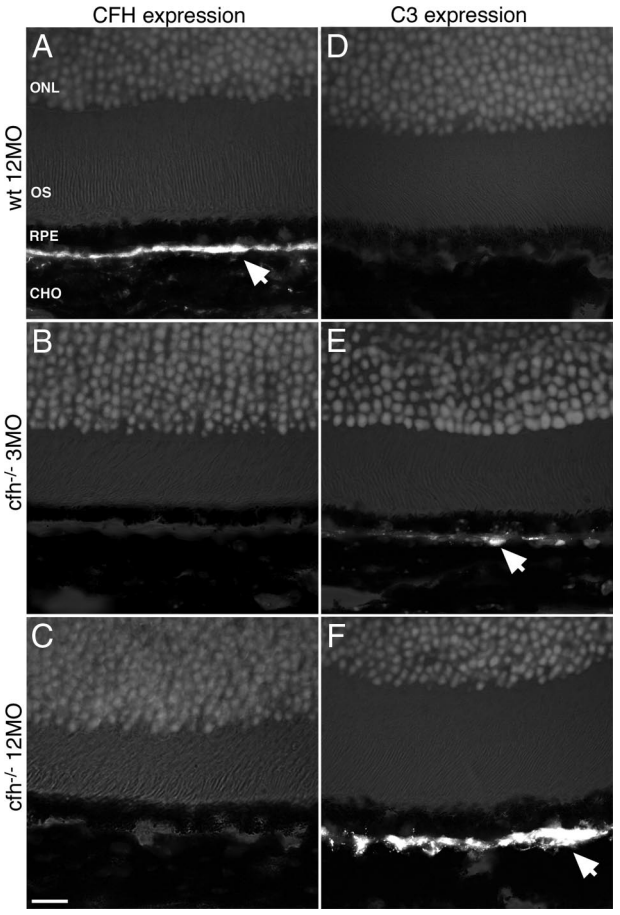

Figure 1. Immunohistochemical analysis of retinal sections shows that CFH expression is predominantly found along the Bruch's membrane in the wild-type mouse, while in the CFH-deficient mouse model C3 deposition accumulates with age on the Bruch's membrane. Shown are representative micrographs from aged control ($n = 5$) (**A** and **D**), 3-month-old ($n = 5$) (**B** and **E**), and 12-month-old $cfh^{-/-}$ ($n = 5$) (**C** and **F**) mice showing outer segment (OS), retinal pigment epithelium (RPE), and Bruch's membrane, which is between the RPE and the choroid (CHO). (BM). Positive staining for CFH (**arrow**) in control mice (**A**) is continuously observed along the Bruch's membrane but is totally absent in both age groups of $cfh^{-/-}$ mice (**B** and **C**). While complement C3 deposition is absent in control mice retinae (**D**), in the 3-month-old $cfh^{-/-}$ animals, C3 is fragmentally deposited adjacent to basal RPE (**arrow** in **E**) and in 1-year-old $cfh^{-/-}$ mice there is a continuous deposition of C3 along the RPE-Bruch's membrane-choroid interface (**arrow** in **F**). Outer nuclear layer, ONL. Scale bar = 20 μm.

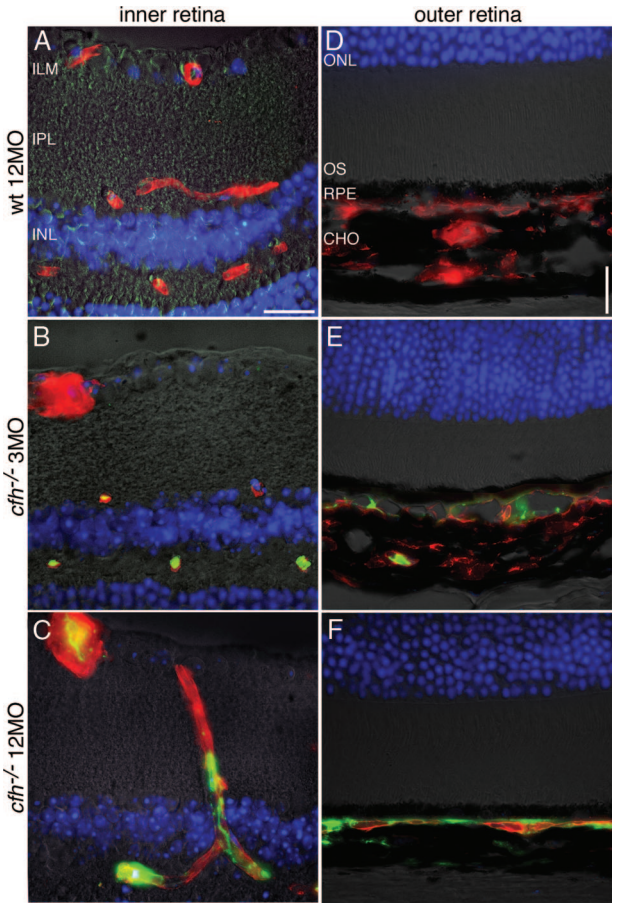

Figure 2. Deposition of C3 along endothelial surfaces in the retina increases with age in the CFH-deficient mouse. Representative micrographs showing immunohistochemical colocalization of C3 deposition (green) and isolectin B4, a vascular endothelium marker (red) in retinae from 3-month-old $cfh^{-/-}$ ($n = 5$), 12-month-old $cfh^{-/-}$ ($n = 5$), and 12-month-old wild-type control mice ($n = 5$) sections. C3 deposition is absent in the inner (**A**) and outer (**D**) retina in the aged wild-type mouse. In the 3-month-old $cfh^{-/-}$ mouse, C3 protein is only detected on the endothelium of the deep microcapillaries in the inner retina outer plexus (**B**); it is also fragmentally deposited in the apical choroid (**E**). However, in the 1-year-old $cfh^{-/-}$ mouse, C3 has accumulated in the majority of endothelial vessel walls in the inner retina (**C**). It has also accumulated along the basal side of the RPE (**F**)—where the Choroidal vasculature has withered away as evidenced by the absence of isolectin-stained endothelium from large parts of the choroid. Inner limiting membrane, ILM; inner plexiform layer, IPL; and inner nuclear layer, INL. Scale bar = 20 μm.

Isolectin staining of the choroidal endothelium revealed a significant reduction in thickness of the vascular bed in this area in the aged $cfh^{-/-}$ animals compared with younger knockout and aged wild-type mice (Figure 2). Surprisingly, the thickness of the choroid, itself, was also significantly reduced in the aged $cfh^{-/-}$ 47.2 ± 2.5 μm compared with the age-matched control 110 ± 7.3 μm and the young knockout 118 ± 7.0 μm ($P < 0.0001$) (Figure 3A).

In whole-mounted preparations of the choriocapillaris it was evident that C3 staining was specific to a subset of blood vessels. Here staining was relatively heavy, while in adjacent vessels no staining was present (Figure 3, B and C). There was no obvious geographic pattern in this feature across the retina. This tendency was also present in inner retinal vessels, although less marked. In the inner retina it appeared around small focal lesions that were commonly adjacent to vascular branch points in young $cfh^{-/-}$ mice (Figure 4, A–D), and was deposited throughout the entire retinal vasculature in 1-year-old $cfh^{-/-}$ animals (Figure 4, E–F).

Sections of upper and lower abdominal aorta, kidney afferent arteriole and glomerulus, lungs, heart and circle of Willis in 1-year-old $cfh^{-/-}$ and age-matched controls were also stained for C3 deposition and consistent $C3^{+}$ was found in lower aorta adjacent to the kidney and the kidney afferent arteriole and glomerulus in the CFH-deficient mouse (data not shown).

Fragmented C3b-expression was found in aged $cfh^{-/-}$ mouse along endothelial surfaces throughout the retina in both cryostat sections and retinal flat mounts and always colocalized with uncleaved C3, however at much reduced levels (Figure 5, A–C). It was present in both

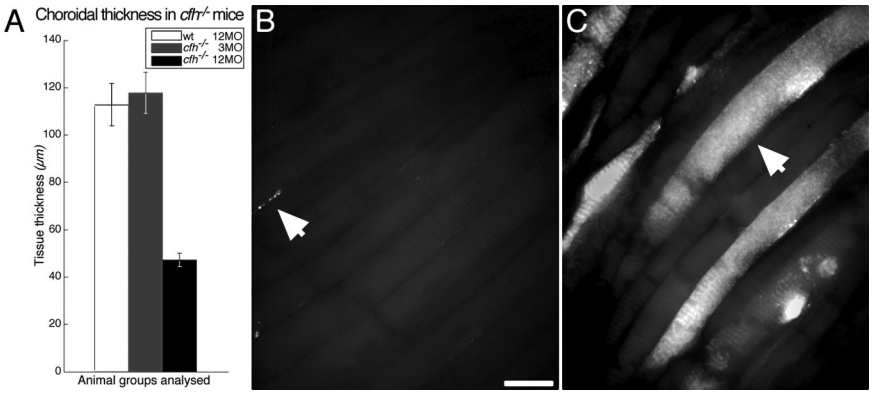

Figure 3. Choroidal thickness at the posterior pole was found to reduce with age in the CFH-deficient mouse and C3 deposition increased compared with wild-type. The choroidal thickness was significantly reduced in the aged $cfh^{-/-}$ mouse compared with that in the age-matched control and the 3-month-old $cfh^{-/-}$ mouse (**A**) ($P < 0.0001$). Choroidal flat mounts revealed almost total absence of C3 deposition in aged wild-type retinae (**arrow** in **B**), while extensive deposition of complement C3 (green) was observed in the aged $cfh^{-/-}$ (**arrow** in **C**). Scale bar = 10 μm.

primary and deep vascular plexuses, as well as, along the Bruch's membrane/choroid interface. C3b depositions were correlated with vascular constrictions in fluorescein angiographs. No $C3b^{+}$ depositions were found in either young CFH-deficient, or aged wild-type retinae.

Fluorescein angiography revealed marked abnormalities in ageing $cfh^{-/-}$ vascular architecture. Fluorescein angiography was used to map capillary networks in the primary and outer plexus of the inner retina. Because of time constraints imposed by its circulation and leakage, vascular quantifications were only made within a 1-mm radius of the optic disk. Fluorescein images showed clear differences in vascular appearance between the control animals and both the young and aged $cfh^{-/-}$ mice. In normally aged and young $cfh^{-/-}$ mice, the plexuses of retinal vessels in both the inner and outer retina was normal (Figure 6, A–F). However, in aged $cfh^{-/-}$ animals there was a significant ($P < 0.001$) withering and reduced density of the capillary network of the outer plexus of the retinal vasculature. Further, there were a significantly large number of local restrictions/venous beads ($P < 0.0001$) apparent on larger calibre veins in the primary plexus (Figure 6, G–J).

Histological evidence from NADPH stained retinal flat mounts that revealed the vascular patterns supported these results, with branch point frequency connecting the primary with the outer plexus in the aged wild-type and 3-month-old $cfh^{-/-}$ mice retinae being substantially

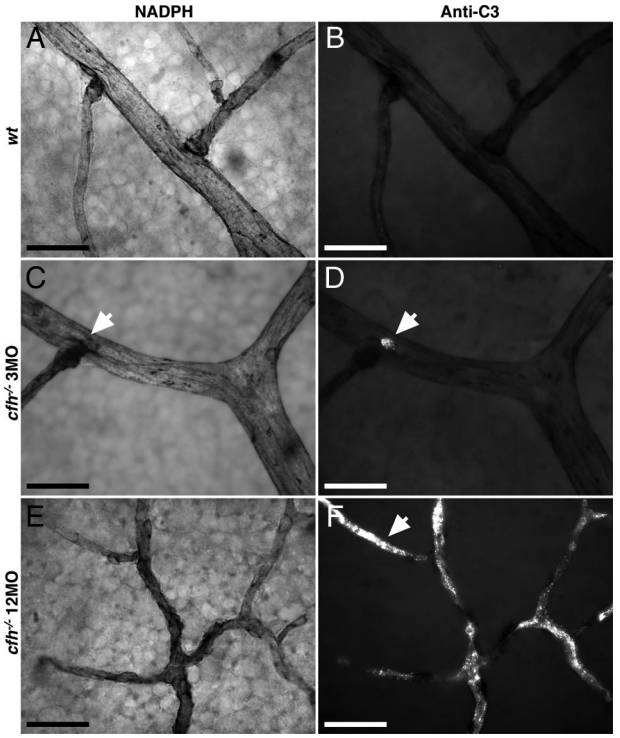

Figure 4. Representative details of vasculature from primary plexus of flat mounted neural retina in 3-month-old ($n = 3$) and 1-year-old ($n = 3$) CFH deficient mice and 1-year-old control animals ($n = 3$) show increased deposition of C3 with age in knockout retina compared with the wild-type. Details of vessels stained with NADPH show the extent of vascular withering in the aged CFH-deficient retina (**E**) compared with those of young $cfh^{-/-}$ (**C**) and aged control retinae (**A**). C3-labeling (**B, D,** and **F**) exhibited extensive C3 accumulation in the aged $cfh^{-/-}$ (**arrow** in **F**) compared with young knockouts (**D**) and aged control animals (**B**). The vascular bed in the 3-month-old $cfh^{-/-}$ mouse retina appears relatively intact, however small ruptures at branching points (**arrows** in **C** and **D**) show small depositions of complement C3. The vascular bed in 1-year-old $cfh^{-/-}$ mice retina has a withered appearance (**E**) and around 80% of it is complement $C3^{+}$ (**F**). Scale bar = 20 μm.

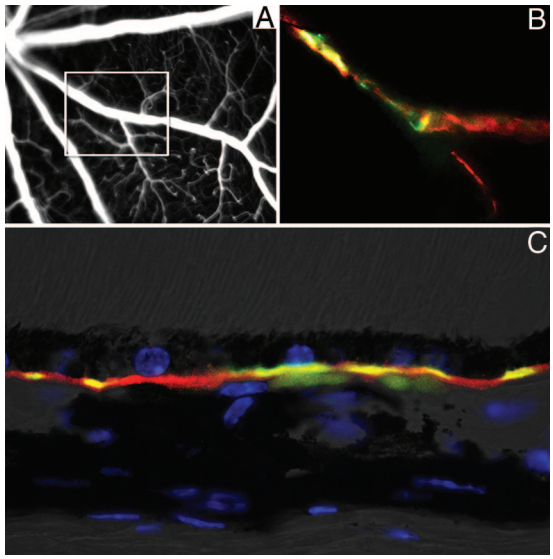

Figure 5. Vascular depositions of activated C3 (C3b) fragments are present both in the inner retinal vasculature and along the Bruch's membrane in the aged CFH-deficient mouse. High-resolution fluorescein angiogram shows venous beading in a 12-month-old $cfh^{-/-}$ (**A**). Detail of flat-mounted retina imaged in (**A**) show colocalized deposition of C3 (red) and C3b (green) (**B**) around vascular beading. Colocalization of inactive and active (C3b) forms of C3 along the Bruch's membrane in the outer retina (**C**).

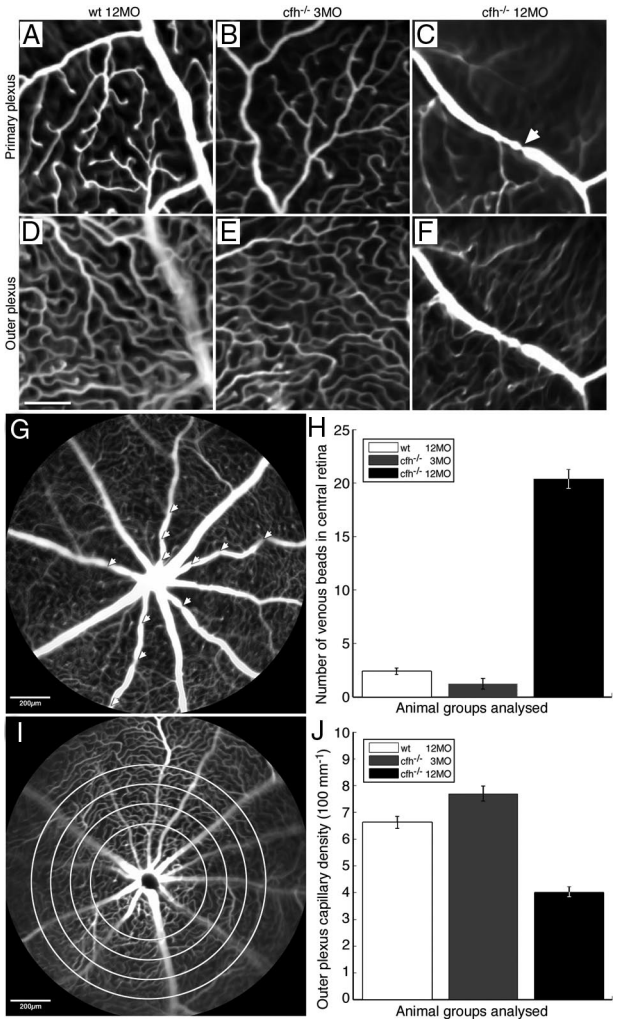

Figure 6. Fluorescein angiographs illustrate vascular abnormalities in the aged CFH-deficient mouse retina compared with the age-matched control and the 3-month-old $cfh^{-/-}$ retina. **A–F** show high-resolution cSLO images of retinal vasculature at the level of the primary plexus (**A–C**) and at the level of the outer plexus (**D–F**) in 12-month-old control mice (**A** and **D**) ($n = 5$), 3-month-old *cfh*/ mice (**B** and **E**) ($n = 4$) and 1-year-old *cfh*/ mice (**C** and **F**) ($n = 6$). Vascular plexuses appear normal in the retina of aged control and 3-month-old $cfh^{-/-}$ mice. However, there is a large presence of venous beading in the primary plexus (**arrow** in **C**) and reduced retinal perfusion in the outer plexus in the retinae of 1-year-old $cfh^{-/-}$ mice. Scale bar = 100 μm. Quantification of vascular abnormalities in these animal groups revealed significant changes in the aged $cfh^{-/-}$ mouse compared with younger mutants and aged control mice. Venous beads (**arrowheads**) from a 1-year-old $cfh^{-/-}$ retina (**G**) in the primary plexus are defined as focal constrictions where the venous diameter is reduced by >40%. One-way analysis of variance analysis showed significantly larger number of venous beads in the primary plexus of the aged $cfh^{-/-}$ compared with the other two groups ($P < 0.0001$) **H:** Vascular perfusion in the outer plexus was quantified using a simple edge detection algorithm, which was applied radially at 100-μm intervals from the optic disk (as indicated by the concentric circles) **I:** Vascular density per 100 μm in the outer plexus was found to be significantly lower in the 1-year-old $cfh^{-/-}$ compared with that of the 3-month-old $cfh^{-/-}$ and 1-year-old control mice using one-way analysis of variance analysis ($P < 0.001$) (**J**).

higher than in aged mutant animals ($P < 0.025$) (data not shown).

The reduced architecture of the retinal circulation in $cfh^{-/-}$ mice was reflected in functional tests of perfusion rates. The arteriovenous phase, a measure of retinal perfusion showed that in mutant mice less fluorescein gets

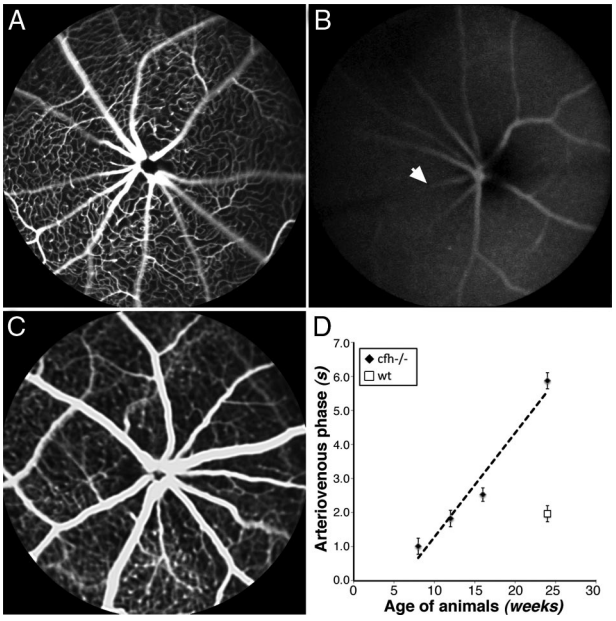

Figure 7. High-frequency retinal fluorescein angiography image sequences show an increase in the arteriovenous perfusion phase time in the 1-year-old $cfh^{-/-}$ mouse compared with the age-matched control. Fluorescein angiograms of the arteriovenous phase at the level of the primary plexus in 6-week-old $cfh^{-/-}$ (**A**), 6-month-old $cfh^{-/-}$ (**B**), and 6-month-old wild-type mouse retina (**C**) illustrate the increased delay in retinal circulation in the aged $cfh^{-/-}$ mouse. This delay is quantified in (**D**) where the arteriovenous phase is plotted as a function age. **Arrow** denotes a vein.

into the retinal arteries and it takes a longer time to clear from the retinal veins (Figure 7, A–D).

A reduction in the volume of vascular leakage was found around laser-induced CNV in 1-year old CFH-deficient mice. The area of laser-induced CNV was similar in aged knockout and control animals. In both animal groups one month after the procedure CNV was present, however, the volume of the neovascularized region was significantly larger in the aged mutants compared with younger or control animals ($P = 0.014$), (data not shown). Despite this difference, fluorescein angiography of photo-lesion induced CNV in 1-year old $cfh^{-/-}$ and age-matched controls revealed a significant reduction in large bleeds in the knockout animals ($P = 0.023$) (Figure 8, A–H). This presumably results from the restricted perfusion in these animals.

FITC- and rhodamine B-conjugated dextran choroidal leakage associated with experimentally induced choroidal neovascularization was measured in the retina in 12-month-old CFH-knockout and age-matched control eyes. Dextran conjugated with a fluorochrome noncovalently binds to plasma albumin in the blood stream and is in case of endothelial damage extravasated into the interstitial space. After clearance of intravascular dextran-fluorochromes, the amount of extravasated dye was extracted from the interstitial space and quantitated. Retinal leakage of rhodamine B-dextran was significantly lower ($P < 0.001$) in the $cfh^{-/-}$ eyes (7.9 ± 2.5 mg/ml per mg retinal tissue) compared with the control retinae (40.6 ± 2.1 mg/ml per mg retinal tissue). Retinal leakage of FITC-dextran was also significantly lower ($P < 0.01$) in the $cfh^{-/-}$ eyes (33.87 ± 8.65 mg/ml per mg retinal

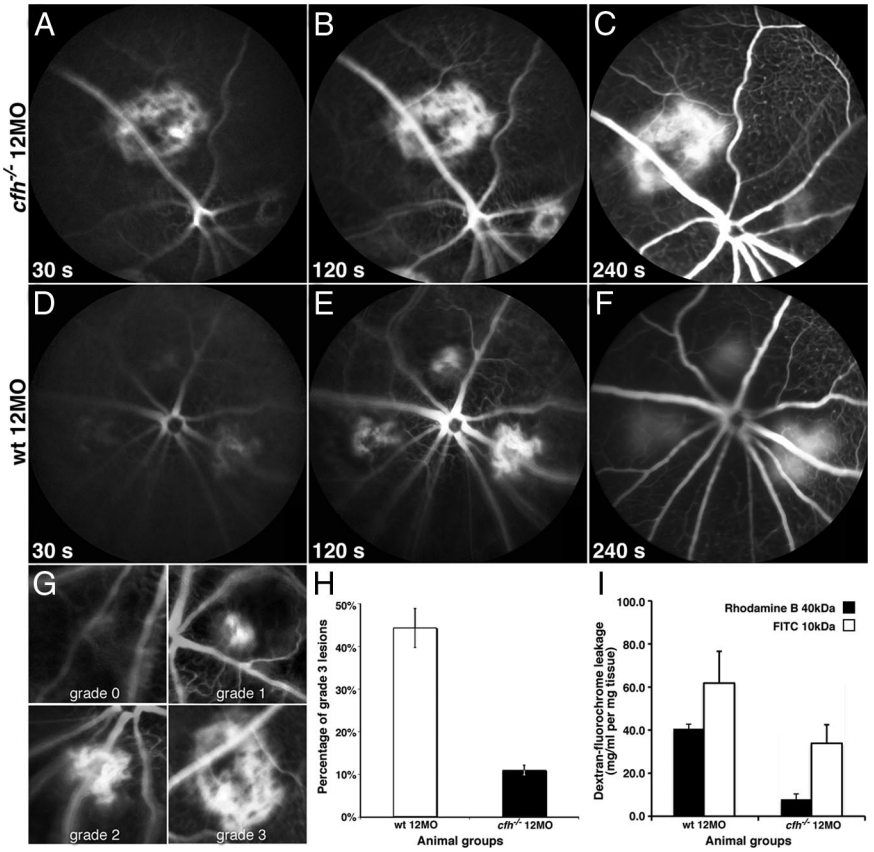

Figure 8. Experimentally induced CNV results in reduced leakage in the aged $cfh^{-/-}$ mouse compared with the aged-matched wild-type. Representative time-lapse fluorescein angiography sequence in 12-month-old complement factor H-deficient and aged-matched control mouse retinae show greater leakage over time in lesioned wild-type retina compared with lesioned CFH-deficient mice retina 2 weeks after procedure (**A–F**). The grading protocol used to compare leakage in experimentally induced CNV in 1-year-old $cfh^{-/-}$ with aged-matched control mice (**G**). Wilcoxon signed-rank test show significant difference in grade three bleeds between 1-year-old $cfh^{-/-}$ ($n = 6$) and aged-matched control mice ($n = 6$) ($P < 0.025$). **H:** Graph illustrating the reduction in leakage from experimentally induced CNV in 1-year-old $cfh^{-/-}$ compared with age-matched control mice 14 days after procedure. Rhodamine B-dextran leakage in knockout retinae (black bars) relative to control retinae normalized for dry weight of the tissue, plasma concentration and endogenous fluorescence and expressed as fluorochrome concentration in mg/ml per mg tissue is significantly smaller ($P < 0.001$). FITC-dextran leakage, similarly quantified is also significantly inferior ($P < 0.01$) to that in age-matched controls. Values are calculated as means ± SEM from $n = 4$ (**I**).

tissue) compared with the control retinae (61.81 ± 14.79 mg/ml per mg retinal tissue) (Figure 8I).

While no evidence was found of complement C5 deposition, abnormal levels of F4/80^{+}, a macrophage specific marker, or expression of C5b-9 in unchallenged aged $cfh^{-/-}$ retinal sections, these markers were all present in and around lesions in experimentally induced CNV retinae. Although the area of CNV at each lesion site was considerably larger in the aged CFH-deficient retinae compared with age-matched controls, the presence of these markers was not substantially higher in knockout mouse (data not shown). However, this could be due to the 14-day interval chosen for CNV evaluation.

Discussion

The *in vivo* data on vascular changes in the retinae of aged $cfh^{-/-}$ mice together with *in situ* immunohistochemistry show that CFH is essential for the long-term health of the vascular endothelium in the murine retina. Thus, in the absence of CFH, we find an accumulation of C3 and C3b protein deposition over time in combination with vascular anomalies. This demonstrates that CFH deficiency, in combination with aging, is directly linked with deposition of C3 on the vascular endothelium in the neural retina and at the RPE-choroid interface. The relationship found in the present study between CFH-deficiency, vascular pathologies, reduced perfusion, and uncleaved and cleaved C3 deposition indicates the systemic importance of CFH rather than, or in combination with, local production of CFH, as previously suggested.[20]

The reduced perfusion in the outer plexus identified in the aged CFH-deficient mouse retina can lead to leukocyte trapping in retinal capillaries, which in combination with endothelial cell hypertrophy, and basement membrane thickening seem to induce increased stress between leukocytes and vascular endothelium, and eventually ischemia in both the inner retina and choroid.[28] Such pathology has been linked to increased vascular endothelial growth factor (VEGF) production[29] that in the context of a thickened endothelial membrane can cause reduced retinal perfusion.[30] Further, evidence of activated C3 acting as a potential promoter of retinal endothelial damage and ischemia inducing mediator was found in preliminary PCR analysis that showed a substantial increase in the $VEGF_{164}/VEGF_{120}$ ratio in 1-year-old CFH-deficient mice compared age-matched controls (private communication M. Semo).

Endothelial cells are the primary source of angiopoetin 2, a protein that promotes angiogenesis and the formation of mature blood vessels, which is released in the early stages after trauma and is directly correlated with complement activation. Angiopoetin 2 acts as a blood vessel destabilizing cytokine, which disrupts the endothelial blood retinal barrier, and as a consequence promotes angiogenesis.[31] The vascular withering occurring in the deep retinal capillary plexus and venular beading of the primary plexus in CFH-deficient mice suggests a

role for the alternative complement system in regulating perfusion in the retina, as well as other heavily vascularized tissues such as those surrounding the renal afferent arteriole and glomerulus.[22,32] There may also be a possible link between it, and up-regulated C3 and $VEGF^{+}$. An additional feature of C3 and C3b depositions studied in the retina was its selectivity, with some vessels showing high levels of deposition, while others that were adjacent showed no deposition of this marker.

The deficiency in complement factor H leads to unregulated activation of the alternative pathway through C3 convertase mediated cleavage. It is therefore no surprise C3b depositions, although fragmented, were colocalized with uncleaved C3 along endothelial surfaces throughout the retina. However, by-products of the complement cascade that would mediate or further promote vascular leakage were absent in aged unchallenged, CFH-deficient retinae. The lack of C5 and C5b depositions in unchallenged aged $cfh^{-/-}$ retinae appears to indicate the presence of an inhibitor, which either blocks activation of the terminal part of the complement cascade through deactivation of an activation fragment, or antagonization of a complement receptor. C5 and C5b depositions were only found in CFH-deficient retinae within and surrounding lesions from laser-induce CNV.

VEGF is a heparin-binding growth factor capable of inducing angiogenesis both *in vitro* and *in vivo*. VEGF is secreted, and its actions are largely confined to endothelial cells. It may promote the up-regulation of the complement-regulatory protein decay-accelerating factor, which is able to reduce C3 vessel binding (a possible explanation for the selective C3 detection). This is considered to be a cytoprotective effect of VEGF.[33] The activation of C5 is critically dependent on an excess of activated C3.

Even without a direct immune challenge, retinal inflammation and potential atrophy appears to occur with age in the absence of CFH, starting with the appearance of vascular abnormalities and pathologies, which suggests that some complement-mediated retinal damage may occur without the need for an external activation of the complement system. It has, for instance, recently been reported that RPE phagocytosis derivatives, directly linked with AMD pathogenesis are sufficient to activate the alternative complement pathway.[34] Consequently, uncontrolled C3 activation due to impairment of the alternative pathway appears to be linked with ischemia-type pathologies in the retinal vasculature.

This study lends additional evidence to previous reports, where it has been demonstrated that homozygous CFH deficiency reproduces some but not all of the hallmarks of AMD. A plausible explanation is that CFH polymorphisms associated with AMD have altered, as opposed to reduced, functions, but factors such as species differences in the innate immune system and the absence of a macula may also prohibit the development of a more pronounced AMD mouse phenotype. A major difference between the CFH polymorphisms associated with human AMD and homozygous deficiency of CFH in the murine model is that in the latter, plasma C3 levels are markedly reduced, while in the former, they are normal.[22] Plasma C3 deficiency may critically influence the ocular phenotype described in $cfh^{-/-}$ mice. For example, C3a blockade improved vascular proliferation in a murine choroidal neovascularization model.[4]

Our data demonstrate that the uncontrolled AP activation in the setting of murine CFH deficiency results in spontaneous and age-related vascular and choroidal pathologies in aged animals. This is consistent with the hypothesis that AMD at-risk CFH polymorphisms are likely to be associated with enhanced AP activation.

Acknowledgments

We thank Coziana Ciurtin (Carol Davila University of Medicine and Pharmacy, Bucharest, Romania), Adnan Tufail (Moorfields Eye Hospital, London, UK), and Ma'ayan Semo (Institute of Ophthalmology, UCL, London, UK) for their helpful suggestions.

References

1. Wang F, Rendahl KG, Manning WC, Quiroz D, Coyne M, Miller SS: AAV-mediated expression of vascular endothelial growth factor induces choroidal neovascularization in rat. Invest Ophthalmol Vis Sci 2003, 44:781–790
2. Bora PS, Hu Z, Tezel TH, Sohn JH, Kang SG, Cruz JM, Bora NS, Garen A, Kaplan HJ: Immunotherapy for choroidal neovascularization in a laser-induced mouse model simulating exudative (wet) macular degeneration. Proc Natl Acad Sci USA 2003, 100:2679–2684
3. Sepp T, Khan JC, Thurlby DA, Shahid H, Clayton DG, Moore AT, Bird AC, Yates JR: Complement factor H variant Y402H is a major risk determinant for geographic atrophy and choroidal neovascularization in smokers and nonsmokers. Invest Ophthalmol Vis Sci 2006, 47:536–540
4. Nozaki M, Raisler BJ, Sakurai E, Sarma JV, Barnum SR, Lambris JD, Chen Y, Zhang K, Ambati BK, Baffi JZ, Ambati J: Drusen complement components C3a and C5a promote choroidal neovascularization. Proc Natl Acad Sci USA 2006, 103:2328–2333
5. Ebrahem Q, Renganathan K, Sears J, Vasanji A, Gu X, Lu L, Salomon RG, Crabb JW, Anand-Apte B: Carboxyethylpyrrole oxidative protein modifications stimulate neovascularization: Implications for age-related macular degeneration. Proc Natl Acad Sci USA 2006, 103: 13480–13484
6. Moore DJ, Hussain AA, Marshall J: Age-related variation in the hydraulic conductivity of Bruch's membrane. Invest Ophthalmol Vis Sci 1995, 36:1290–1297
7. Spraul CW, Lang GE, Grossniklaus HE: Morphometric analysis of the choroid. Bruch's membrane, and retinal pigment epithelium in eyes with age-related macular degeneration. Invest Ophthalmol Vis Sci 1996, 37:2724–2735
8. Hollyfield JG, Bonilha VL, Rayborn ME, Yang X, Shadrach KG, Lu L, Ufret RL, Salomon RG, Perez VL: Oxidative damage-induced inflammation initiates age-related macular degeneration. Nat Med 2008, 14:194–198
9. Klein RJ, Zeiss C, Chew EY, Tsai JY, Sackler RS, Haynes C, Henning AK, SanGiovanni JP, Mane SM, Mayne ST, Bracken MB, Ferris FL, Ott J, Barnstable C, Hoh J: Complement factor H polymorphism in age-related macular degeneration. Science 2005, 308:385–389
10. Hageman GS, Anderson DH, Johnson LV, Hancox LS, Taiber AJ, Hardisty LI, Hageman JL, Stockman HA, Borchardt JD, Gehrs KM, Smith RJ, Silvestri G, Russell SR, Klaver CC, Barbazetto I, Chang S, Yannuzzi LA, Barile GR, Merriam JC, Smith RT, Olsh AK, Bergeron J, Zernant J, Merriam JE, Gold B, Dean M, Allikmets R: A common haplotype in the complement regulatory gene factor H (HF1/CFH) predisposes individuals to age-related macular degeneration. Proc Natl Acad Sci USA 2005, 102:7227–7232
11. Gold B, Merriam JE, Zernant J, Hancox LS, Taiber AJ, Gehrs K, Cramer K, Neel J, Bergeron J, Barile GR, Smith RT, Hageman GS, Dean M, Allikmets R: Variation in factor B (BF) and complement

component 2 (C2) genes is associated with age-related macular degeneration. Nat Genet 2006, 38:458–462
12. Magnusson KP, Duan S, Sigurdsson H, Petursson H, Yang Z, Zhao Y, Bernstein PS, Ge J, Jonasson F, Stefansson E, Helgadottir G, Zabriskie NA, Jonsson T, Bjornsson A, Thorlacius T, Jonsson PV, Thorleifsson G, Kong A, Stefansson H, Zhang K, Stefansson K, Gulcher JR: CFH Y402H confers similar risk of soft drusen and both forms of advanced AMD. PLoS Med 2006, 3:e5
13. Despriet DD, Klaver CC, Witteman JC, Bergen AA, Kardys I, de Maat MP, Boekhoorn SS, Vingerling JR, Hofman A, Oostra BA, Uitterlinden AG, Stijnen T, van Duijn CM, de Jong PT: Complement factor H polymorphism, complement activators, and risk of age-related macular degeneration. JAMA 2006, 296:301–309
14. Tuo J, Ning B, Bojanowski CM, Lin ZN, Ross RJ, Reed GF, Shen D, Jiao X, Zhou M, Chew EY, Kadlubar FF, Chan, CC: Synergic effect of polymorphisms in ERCC6 5′ flanking region and complement factor H on age-related macular degeneration predisposition. Proc Natl Acad Sci USA 2006, 103:9256–9261
15. Johnson PT, Betts KE, Radeke MJ, Hageman GS, Anderson DH, Johnson, LV: Individuals homozygous for the age-related macular degeneration risk-conferring variant of complement factor H have elevated levels of CRP in the choroid. Proc Natl Acad Sci USA 2006, 103:17456–17461
16. Hughes AE, Orr N, Esfandiary H, Diaz-Torres M, Goodship T, Chakravarthy U: A common CFH haplotype, with deletion of CFHR1 and CFHR3, is associated with lower risk of age-related macular degeneration. Nat Genet 2006, 38:1173–1177
17. Maller J, George S, Purcell S, Fagerness J, Altshuler D, Daly MJ, Seddon JM: Common variation in three genes, including a noncoding variant in CFH, strongly influences risk of age-related macular degeneration. Nat Genet 2006, 38:1055–1059
18. Francis PJ, Schultz DW, Hamon S, Ott J, Weleber RG, Klein ML: Haplotypes in the complement factor H (CFH) gene: associations with drusen and advanced age-related macular degeneration. PLoS ONE 2007, 2:e1197
19. Hughes AE, Orr N, Patterson C, Esfandiary H, Hogg R, McConnell V, Silvestri G, Chakravarthy U: Neovascular age-related macular degeneration risk based on CFH. LOC387715/HTRA1, and smoking. PLoS Med 2007, 4:e355
20. Thurman JM, Holers VM: The central role of the alternative complement pathway in human disease. J Immunol 2006, 176:1305–1310
21. Pickering MC, Cook HT, Warren J, Bygrave AE, Moss J, Walport MJ, Botto M: Uncontrolled C3 activation causes membranoproliferative glomerulonephritis in mice deficient in complement factor H. Nat Genet 2002, 31:424–428
22. Noris M, Remuzzi G: Complement factor h gene abnormalities in haemolytic uraemic syndrome: from point mutations to hybrid gene. PLoS Med 2006, 3:e432
23. Coffey PJ, Gias C, McDermott CJ, Lundh von Leithner P, Pickering MC, Sethi C, Bird A, Fitzke FW, Maass A, Holder GE, Luthert PJ, Salt TE, Moss SE, Greenwood J: Complement factor H-deficiency in aged mice causes retinal abnormalities and visual dysfunction. Proc Natl Acad Sci USA 2007, 104:16651–16656
24. Ishida S, Usui T, Yamashiro K, Kaji Y, Ahmed E, Carrasquillo KG, Amano S, Hida T, Oguchi Y, Adamis AP: VEGF164 is proinflammatory in the diabetic retina. Invest Ophthalmol Vis Sci 2003, 44:2155–2162
25. Schwesinger C, Yee C, Rohan RM, Joussen AM, Fernandez A, Meyer TN, Poulaki V, Ma JJ, Redmond TM, Liu S, Adamis AP, D'Amato RJ: Intrachoroidal neovascularization in transgenic mice overexpressing vascular endothelial growth factor in the retinal pigment epithelium. Am J Pathol 2001, 158:1161–1172
26. Takemura M, Wakisaka S, Iwase K, Yabuta NH, Nakagawa S, Chen K, Bae YC, Yoshida A, Shigenaga Y: NADPH-diaphorase in the developing rat: lower brainstem and cervical spinal cord, with special reference to the trigemino-solitary complex. J Comp Neurol 1996, 365:511–525
27. Takehana Y, Kurokawa T, Kitamura T, Tsukahara Y, Akahane S, Kitazawa M, Yoshimura N: Suppression of laser-induced choroidal neovascularization by oral tranilast in the rat. Invest Ophthalmol Vis Sci 1999, 40:459–466
28. Hofman P, van Blijswijk BC, Gaillard PJ, Vrensen GF, Schlingemann RO: Endothelial cell hypertrophy induced by vascular endothelial growth factor in the retina: new insights into the pathogenesis of capillary nonperfusion. Arch Ophthalmol 2001, 119:861–866
29. Ng EW, Adamis AP: Targeting angiogenesis, the underlying disorder in neovascular age-related macular degeneration. Can J Ophthalmol 2005, 40:352–368
30. Schmid-Schonbein GW, Engler RL: Perspectives of leukocyte activation in the microcirculation. Biorheology 1990, 27:859–869
31. Hunigen H, Bisplinghoff P, Plendl J, Bahramsoltani, M: Vascular dynamics in relation to immunolocalisation of VEGF-A, VEGFR-2 and Ang-2 in the bovine corpus luteum. Acta Histochem 2008, 110:462–472
32. Abrera-Abeleda MA, Xu Y, Pickering MC, Smith RJ, Sethi S: Mesangial immune complex glomerulonephritis due to complement factor D deficiency. Kidney Int 2007, 71:1142–1147
33. Mason JC, Lidington EA, Ahmad SR, Haskard DO: bFGF and VEGF synergistically enhance endothelial cytoprotection via decay-accelerating factor induction. Am J Physiol Cell Physiol 2002, 282: C578–C587
34. Zhou J, Jang YP, Kim SR, Sparrow JR: Complement activation by photooxidation products of A2E, a lipofuscin constituent of the retinal pigment epithelium. Proc Natl Acad Sci USA 2006, 103:16182–16187